

**Use of phase change materials (PCMs) to mitigate early age thermal cracking in concrete  
Theoretical considerations**

Savija, Branko; Schlangen, Erik

**DOI**

[10.1016/j.conbuildmat.2016.09.046](https://doi.org/10.1016/j.conbuildmat.2016.09.046)

**Publication date**

2016

**Document Version**

Accepted author manuscript

**Published in**

Construction and Building Materials

**Citation (APA)**

Savija, B., & Schlangen, E. (2016). Use of phase change materials (PCMs) to mitigate early age thermal cracking in concrete: Theoretical considerations. *Construction and Building Materials*, 126, 332-344. <https://doi.org/10.1016/j.conbuildmat.2016.09.046>

**Important note**

To cite this publication, please use the final published version (if applicable).  
Please check the document version above.

**Copyright**

Other than for strictly personal use, it is not permitted to download, forward or distribute the text or part of it, without the consent of the author(s) and/or copyright holder(s), unless the work is under an open content license such as Creative Commons.

**Takedown policy**

Please contact us and provide details if you believe this document breaches copyrights.  
We will remove access to the work immediately and investigate your claim.

1           **Use of phase change materials (PCMs) to mitigate early age thermal**  
2                           **cracking in concrete: theoretical considerations**

3   Branko Šavija<sup>1\*</sup> and Erik Schlangen<sup>1</sup>

4           1- Microlab, Faculty of Civil Engineering and Geosciences, Delft University of Technology  
5   Stevinweg 1, 2628 CN Delft, the Netherlands  
6   e-mail: [b.savija@tudelft.nl](mailto:b.savija@tudelft.nl); [erik.schlangen@tudelft.nl](mailto:erik.schlangen@tudelft.nl)

7  
8   \*- corresponding author, Tel: +31(0)15 27 88986, Fax: +31(0)15 27 86383  
9   Article to be submitted to *CONSTRUCTION AND BUILDING MATERIALS*

10  
11   **Abstract**

12   Phase change materials (PCMs) have found their use in concrete technology for increasing energy  
13   efficiency of building envelopes. In recent years, however, new potential applications for PCMs in  
14   concrete have been suggested, for example for reducing freeze-thaw damage and melting of ice  
15   forming on top of concrete pavements. A recent application of PCMs in concrete technology is their  
16   use for mitigating early-age cracking in hydrating concrete. The focus on this paper is therefore on  
17   theoretical considerations related to this particular application of phase change materials. In particular,  
18   the focus is on simulating microencapsulated PCMs, which show very promising experimental  
19   results. Numerical models are developed for 2 scales: the meso-scale, in which the PCM  
20   microcapsules are simulated as discrete inclusions in the cementitious matrix; and the macro-scale,  
21   where the effect of PCM microcapsule addition is considered in a smeared way. On the meso-scale,  
22   the effect of PCM volume percentage, their phase change temperature, and latent heat of fusion on  
23   simulated adiabatic heat evolution are assessed. On the macro-scale, influence of these parameters on  
24   the temperature evolution in semi-adiabatic (field) conditions and tensile stress development are  
25   simulated. The outcomes of this study provide valuable insights related to the influence of PCM  
26   microcapsule parameters on the behaviour of cementitious materials, enabling tailoring composites for  
27   different environmental conditions.

28   **Keywords:** Phase Change Materials (PCMs); Heat evolution; Thermal cracking; Numerical  
29   modelling; Lattice modelling

## 32 **1. Introduction**

33 During construction, temperature in concrete will increase due to exothermic hydration reactions of  
34 cement. If unrestrained, the concrete in a structural element expands and contracts during the early-age  
35 heating and the subsequent cooling process without stresses being induced [1]. In practice, however,  
36 the concrete is nearly always restrained to some degree, either externally by adjoining structures or  
37 internally by different temperatures in the components of the structure itself [1]. This is an issue  
38 especially in massive hardening concrete structures which are most prone to thermal cracking at early  
39 age due to the hydration heat of cement [2-4]. As the surface of the structure will lose heat to the  
40 atmosphere, a thermal gradient will appear between the cold outside and the warm core of the structure  
41 or element. Differences in free thermal dilation between various parts of the structure will give rise to  
42 tensile stresses at the surface [5]. If these stresses exceed the tensile strength of concrete, cracking will  
43 occur. This is a common problem in engineering practice, and may be aggravated by unfavourable  
44 environmental conditions during concrete casting and curing [6]. Definition of mass concrete is  
45 somewhat ambiguous, with ACI 116R defining it as “any volume of concrete with dimensions large  
46 enough to require that measures be taken to cope with generation of heat from hydration of the cement  
47 and attendant volume change, to minimize cracking”[7]. Different agencies give more specific  
48 guidelines, such as defining any concrete element having a least dimension greater than 0.9 m as mass  
49 concrete [8]. Currently, mass concrete is no longer considered only for dam construction; it is also  
50 used for foundation and members of structures for many classes as multistorey and nuclear reactor  
51 buildings [9, 10].

52 Cracks occurring at early age do not necessarily pose a threat to structural safety. However, these  
53 cracks can increase the susceptibility of the structure to environmental attacks, such as chloride ingress  
54 [11, 12]. This can result in a significant reduction of the service life [13]. The occurrence of thermal  
55 cracks depends, in general, on 3 groups of factors [14]: (1) material factors, which are related to mix  
56 proportions, cement type, and admixtures used; (2) structural factors, related mainly to internal and  
57 external restraints on the structure/element; and (3) execution factors, related to placing temperature,

58 curing, insulation, etc. Therefore, different measures can be used to tackle this issue, ranging from  
59 simple changes in mix design (e.g. using lower cement content [4] or blended cements [15]), structural  
60 modifications (e.g. expansion joints, additional reinforcement, prestressing [4, 14]), or execution  
61 parameters (cooling pipes or formwork) [16].

62 Another possibility for mitigating thermal cracking in hardening concrete has been recently proposed  
63 – the use of phase change materials (PCMs) as additives [17-20]. A phase change material has high  
64 heat of fusion which can, by melting and solidifying at a certain temperature, store and dissipate large  
65 amounts of energy in the form of heat [21]. In recent years, many studies have been devoted to the use  
66 of PCMs in cementitious materials to increase the energy efficiency of buildings [22-25]. Different  
67 ways of incorporating PCMs into concrete have been proposed: (1) impregnation in lightweight  
68 aggregates [17, 26, 27]; (2) microencapsulation [19, 24, 28, 29]; and (3) embedding in tubes [26, 30].  
69 In this work, microencapsulated PCMs are considered.

70 Numerical simulation tools have also been proposed in the literature to assess the thermal performance  
71 and the efficiency of PCM modified concrete [31, 32]. The use of modelling tools can help in tailoring  
72 efficient PCM based composites. This study aims to evaluate the effects of adding microencapsulated  
73 PMCs in cement based systems on their thermal and structural performance. First, a meso-scale  
74 numerical tool for simulating temperature evolution in a composite system containing  
75 microencapsulated PCM is presented. This part focuses on material parameters related to PCM  
76 addition, such as the addition percentage, heat of fusion, and temperature of phase change. The next  
77 part deals with modelling of a full-scale hardening concrete structure using a commercial FE package,  
78 where the interaction of the structure with the environment is considered. The main focus of the  
79 second part is to assess the effect of PCM addition on stress evolution in the hardening structure. The  
80 influence of different parameters on temperature and stress development is discussed. This study will  
81 serve as a basis for design and development of PCM modified cement based materials and structures  
82 for mitigating thermal cracking in various environmental conditions.

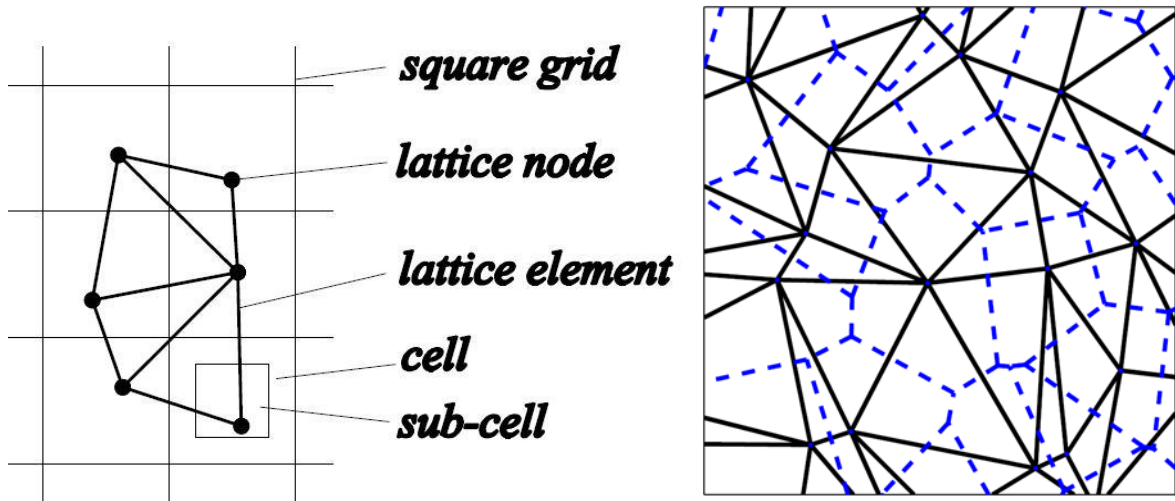
## 83        **2. Methods**

### 84        **2.1. Meso-scale modelling approach**

85        Lattice models have long been used to simulate fracture processes in concrete [33-35] and other quasi-  
86        brittle materials [36, 37]. Unlike the continuum mechanics approaches, in this type of models the  
87        continuum is discretized as a set of two-node (truss or beam) elements which can transfer forces.  
88        Fracture is simulated by damaging these discrete elements. These models can be successfully used on  
89        multiple scales, from the micro-scale (i.e. cement paste scale [38]), to the meso-scale (i.e. mortar scale  
90        [35, 39]) and the macro-scale (i.e. concrete element and structure scale [40]). Different scales can be  
91        simulated in a straight-forward fashion by implementing the material structure appropriate for each  
92        scale.

93        Recently, the concept of lattice (or rather discrete) modelling has been extended to simulating  
94        transport processes in concrete, such as moisture [41, 42] transport, chloride transport [43-45], and  
95        electrical current flow [46]. In the transport model, the material domain is discretized as a set of one-  
96        dimensional “pipe” elements through which the transport takes place. This type of model is used  
97        herein.

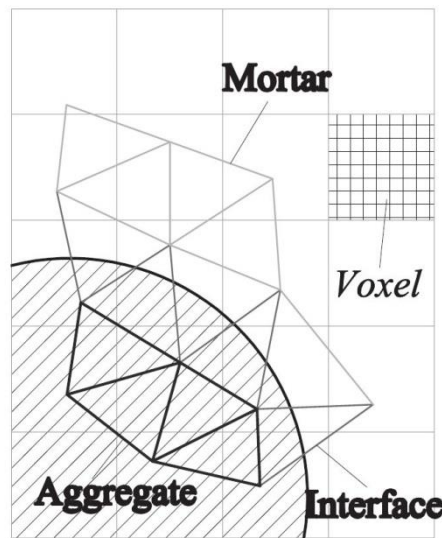
98        For spatial discretization in three dimensions, the starting point is a prismatic domain. This domain is  
99        first divided into a number of cubic cells. Then, a sub-cell is defined in the centre of each cell. A node  
100        is randomly placed within each sub-cell using a pseudo-random number generator (Figure 1). Then, a  
101        Voronoi tessellation of the domain, with respect to the generated set of nodes, is performed. Nodes  
102        with adjacent Voronoi cells are connected by lattice elements (Figure 1) [40].



103

104 **Figure 1.** Left: Node placement procedure in two-dimensions. Right: Meshing procedure in two-dimensions. Solid, lattice;  
 105 dashed, Voronoi cells.

106 Heterogeneous material behaviour can be considered by employing the particle overlay procedure  
 107 (Figure 2). This way, properties can be assigned to different material phases. As an input, either a  
 108 computer generated material structure, or a material structure obtained by scanning (2D) or CT-  
 109 scanning (3D), can be used. Each node in the mesh is assigned with a pixel/voxel value (2D and 3D,  
 110 respectively) from the used material structure. Properties assigned to each element depend on the  
 111 pixel/voxel value at its end nodes (Figure 2).



112

113 **Figure 2.** Particle overlay procedure in two dimensions

114 **2.1.1. Heat transport model**

115 To simulate the heat transport on this scale, the transient heat conduction equation for a stationary  
 116 medium is used [47]:

$$\rho c_p \frac{\partial T}{\partial t} = \frac{\partial}{\partial x} \left( k \frac{\partial T}{\partial x} \right) + \dot{Q} \quad (1)$$

117

118 Here,  $\rho$  is the density (kg/m<sup>3</sup>),  $c_p$  the specific heat capacity (J/kg·K),  $k$  the thermal conductivity  
 119 (W/mK),  $T$  the temperature (K),  $t$  time (s), and  $x$  the spatial coordinate (m). The rate of heat production  
 120 due to hydration is implemented through the source term  $\dot{Q}$  (J/m<sup>3</sup>s).

121 Equation (1) can be discretized in space using the standard Galerkin procedure [43, 47]. The following  
 122 set of equation arises (in matrix form):

$$C \frac{\partial T}{\partial t} + KT = f \quad (2)$$

123

124 In equation (2),  $C$  is the element capacitance matrix,  $K$  the element conductivity matrix, and  $f$  the  
 125 forcing vector. Vector of unknowns,  $T$ , is the vector of temperatures in the nodes of a lattice element.  
 126 Elemental matrices in equation (2) have the following form:

$$C = \frac{Al\rho c_p}{6\omega} \begin{bmatrix} 2 & 1 \\ 1 & 2 \end{bmatrix} \quad (3)$$

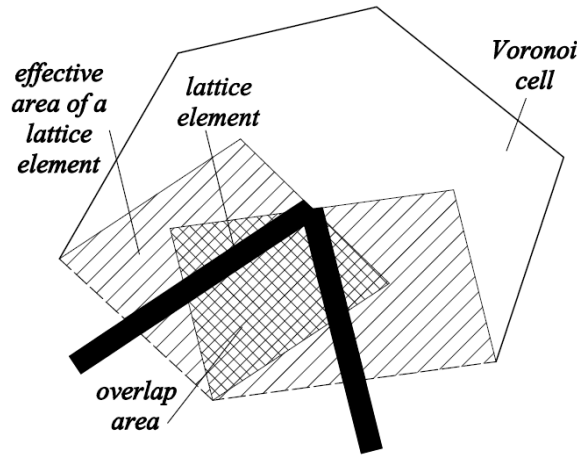
$$K = \frac{kA}{l} \begin{bmatrix} 1 & -1 \\ -1 & 1 \end{bmatrix} \quad (4)$$

127

128 Here,  $l$  is the element length,  $A$  the element cross-sectional area. In the lattice approach, cross-sectional  
 129 areas of individual lattice elements are assigned using the so-called Voronoi scaling method [40, 41] –  
 130 cross sectional area of an element is equal to the area of a facet of a Voronoi cell which is common to  
 131 its end nodes. Note that element capacitance and conductivity matrices are equivalent to those of  
 132 regular 1D linear finite elements [47], except the non-dimensional correction parameter  $\omega$  in the  
 133 capacitance matrix (equation (3)). This parameter is used to convert the volume of a Voronoi cell to  
 134 the volume of lattice elements, due to overlap of volume of adjacent lattice elements (Figure 3). It can  
 135 be calculated as [48]:

$$\omega = \frac{\sum_{k=1}^m A_k \cdot l_k}{V} \quad (5)$$

136 where  $m$  is the total number of elements in the mesh,  $A_k$  and  $l_k$  cross sectional area and length of each  
 137 lattice element,  $k$  element number, and  $V$  the volume of the specimen. It was shown that  $\omega$  can be set  
 138 as 2 for the two-dimensional and 3 for the three-dimensional case, respectively, without loss of  
 139 accuracy [41].



140

141

**Figure 3.** Definition of overlap area for determination of parameter  $\omega$  (adapted from [48]).

142

143

144

The forcing vector, at this scale, considers only the internal development of hydration heat. Heat of hydration calculations are performed for each node using the volume of the corresponding Voronoi cell [6]. Therefore, forcing vector due to heat of hydration for each node is:

$$f_i = \dot{Q}V_i \quad (6)$$

145

146

where  $i$  is the node number, and  $V_i$  the volume of the corresponding Voronoi cell. System matrices are assembled using the standard finite element procedure [47].

147

148

149

150

151

152

The total heat absorbed by PCM microcapsules comprises a sensible heat contribution (proportional to the mass and the specific heat capacity of the material) and the latent heat contribution (proportional to the mass and the enthalpy of phase change) [19]. Most materials can absorb sensible heat: it is the latent heat contribution that provides the PCMs with their energy storage capacity. The latent heat stored during phase change in the PCM microcapsules is taken into account in the model by using the heat capacity method [23]. Contribution from the latent heat due to the phase change process is

153 considered by using a piecewise temperature dependent function for the specific heat capacity of the  
 154 PCM microcapsules [32, 49]:

$$c_p(T) = \begin{cases} c_{p,s} & \text{for } T < T_{pc} - \Delta T_{pc} / 2 \\ c_{p,s} + \frac{h_f}{\Delta T_{pc}} & \text{for } T_{pc} - \Delta T_{pc} / 2 \leq T \leq T_{pc} + \Delta T_{pc} / 2 \\ c_{p,l} & \text{for } T > T_{pc} + \Delta T_{pc} / 2 \end{cases} \quad (7)$$

155  
 156 where  $c_{p,s}$  and  $c_{p,l}$  are the specific heat capacities of the solid and the liquid phase (it is assumed in all  
 157 analyses that  $c_{p,s}=c_{p,l}$ ),  $T_{pc}$  the phase change temperature,  $\Delta T_{pc}$  the temperature window, and  $h_f$  the  
 158 latent heat of fusion of the phase change material.

159 System of equations (2) is discretized in time using the Crank-Nicholson procedure [47]:

$$(C^{n-1} + 0.5\Delta t K)T^n = (C^{n-1} - 0.5\Delta t K)T^{n-1} + \Delta t \cdot f \quad (8)$$

160 This equation is then solved for each discrete time step ( $\Delta t$ ) and the temperature distribution is  
 161 obtained. Since the specific heat capacity ( $c_p$ ) and, therefore, matrix  $C$  is dependent on temperature  $T$   
 162 (for phase change microcapsules, see equation (7)), the iterative procedure is avoided by calculating  
 163 temperature in each step ( $n$ ) based on values of specific heat capacities from the previous step ( $n-1$ ).  
 164 Although this implies a certain amount of error, it significantly shortens the simulation time and the  
 165 error is small for small time step  $\Delta t$ .

166 On the meso-scale, the material is considered to comprise a cementitious matrix and discrete  
 167 microcapsules containing phase-change materials.

### 168 2.1.2. Model validation

169 For the validation of the discrete modelling approach, a homogeneous cement paste specimen was  
 170 simulated. Material properties of the cement paste used in this simulation were given by Thiele et al.  
 171 [32] (see Table 1).

172

173

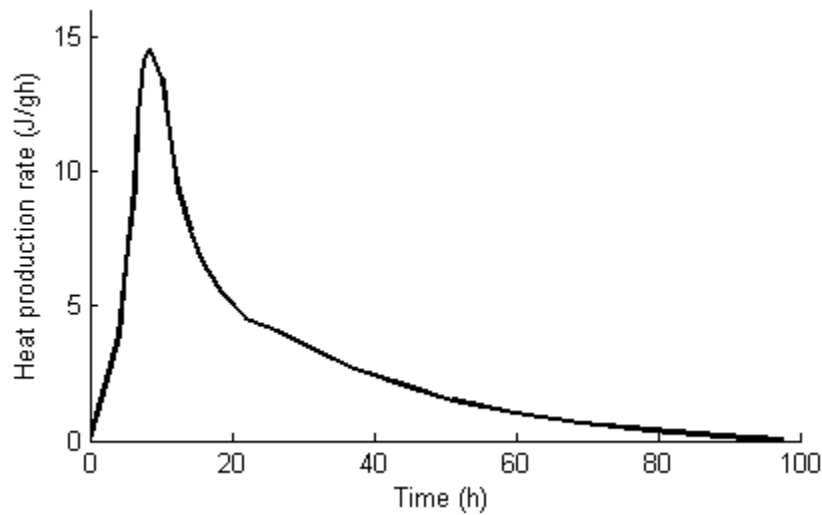
174  
175

**Table 1.** Material properties used in meso-scale simulations [32]. (Note that the PCM used in [32] was an organic paraffin encapsulated by a melamine-formaldehyde shell)

Material	$\rho$ (kg/m <sup>3</sup> )	$c$ (J/kg K)	$k$ (W/mK)
Cement paste	1965	1530	1
PCM	900	1900	0.42

176

177 For the development of heat of hydration, experimental results of De Schutter and Taerwe [50] are  
178 used<sup>1</sup>. They performed isothermal hydration tests for Portland Cement CEM I 52.5. One of their  
179 measurements (at 35 °C) is used herein (Figure 4). The simulated cement paste was assumed to have a  
180 0.45 w/c ratio, which amounts to around 1300 kg/m<sup>3</sup> of cement (assuming specific gravity of 3.15).



181

**Figure 4.** Heat production rate of Portland Cement CEM I 52.5 at 35 °C [50].

182

183 The measured heat production rate was first converted to volumetric heat production rate, and then  
184 applied as the source term according to equation (6).

185 For validation, a homogeneous 30x30x30  $\mu\text{m}^3$  lattice was generated. Cell size of 1x1x1  $\mu\text{m}^3$  with a  
186 sub-cell of 0.5x0.5x0.5  $\mu\text{m}^3$  was used for mesh generation (see Figure 1), with 27000 lattice nodes in  
187 total. Nodes at the domain edges were positioned exactly at the edge, in order to retain the total  
188 volume of the specimen (Figure 5). Adiabatic conditions were assumed (i.e. no heat exchange with the

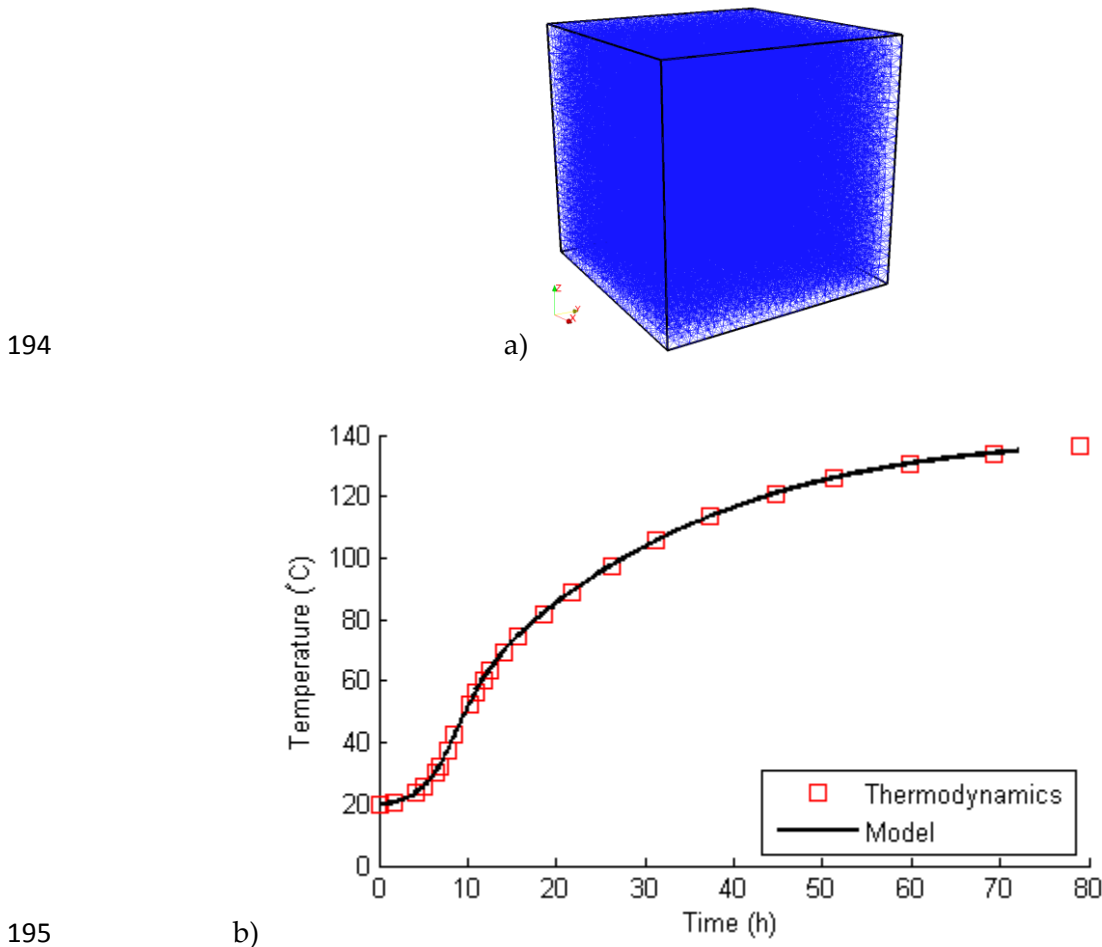
---

<sup>1</sup> This particular heat production rate curve was selected due to its steep increase, because it may be assumed that concrete which exhibits a rapid heat evolution will have a higher risk of thermal cracking. In fact, any heat production curve, be it experimental (e.g. other curves in the paper of De Schutter and Taerwe [50]) or simulated (e.g. by HYMOSTRUC model [51, 52]), can be used in the model.

189 environment occurs)<sup>2</sup>. The initial temperature of the cement paste was assumed as 20°C (293.15K).  
 190 According to the second law of thermodynamics, it is possible to predict the the temperature rise due  
 191 to heat production as [29]:

$$\delta T = \frac{\delta Q \cdot MC}{\rho \cdot c_p} \quad (9)$$

192 where  $\delta T$  is the temperature difference caused by an increment in heat production  $\delta Q$  and  $MC$  the mass  
 193 of cement. In figure 5, simulation results are compared with those obtained using equation (9).



195  
 196 **Figure 5.** (a) A 30x30x30 $\mu\text{m}^3$  random lattice used for model validation; (b) Comparison of the simulated temperature  
 197 evolution and thermodynamic calculations

198 It can be seen in Figure 5 that there is no significant difference between the result of the lattice model  
 199 and the theoretical (i.e. thermodynamics) solution. From this simple example, it can be concluded that  
 200 the model does not show any significant numerical noise due to the lattice randomness.

<sup>2</sup> It should be noted that adiabatic tests are, in practice, performed mostly on concrete, not cement paste. In semi-adiabatic tests of Portland cement paste samples, temperatures close to 100°C have been recorded [53]. For comparison, a simulation of adiabatic temperature rise in concrete is given in the Appendix.

## 201        **2.2. Structural modelling approach**

202 Cracks in hardening concrete do not occur only due to material properties. Even more important is the  
203 structure itself [54]. Temperature induced deformations of a structure can be restrained by already  
204 hardened parts of the structure, leading to cracking. In that case, the rate of heating and cooling of the  
205 structure (together with the mechanical properties of the hardening material) will determine if cracking  
206 will occur.

207 On the structural scale, the influence of PCM additions on the risk of early-age cracking is assessed on  
208 the macro (i.e. structural) scale. Commercial finite element package FEMMASSE is used to simulate  
209 temperature evolution and stress distribution at this scale. FEMMASSE is a finite element model  
210 based on the state parameter concept [54, 55]. That means that the material properties are a function of  
211 the state of the material. The state can be maturity, degree of hydration, temperature, or moisture  
212 potential. On the macro scale, concrete is assumed to be homogeneous and isotropic (i.e. PCM  
213 microcapsules are not explicitly modelled). Instead, the heat absorbing capacity of PCM  
214 microcapsules is included in the concrete material.

### 215        **2.2.1. Heat transport model**

216 Heat transport in FEMMASSE is also simulated using equation 1. For the latent heat contribution  
217 during of the PCM material, also on this scale the heat capacity method is used [23, 49]:

$$\rho c_{p,c}(T) = \begin{cases} \rho c_{p,c} & \text{for } T < T_{pc} - \Delta T_{pc} / 2 \\ \rho c_{p,c} + \frac{h_f \cdot m_{pcm}}{\Delta T_{pc}} & \text{for } T_{pc} - \Delta T_{pc} / 2 \leq T \leq T_{pc} + \Delta T_{pc} / 2 \\ \rho c_{p,c} & \text{for } T > T_{pc} + \Delta T_{pc} / 2 \end{cases} \quad (10)$$

218 where  $c_{p,c}$  is the specific heat capacity of concrete, and  $m_{pcm}$  the quantity of PCM microcapsules per  
219 cubic meter of the mixture. For simplicity, it was assumed that the addition of phase change  
220 microcapsules does not cause a change in density, thermal conductivity, or specific heat capacity  
221 (except due to the latent heat) of the hardening concrete.

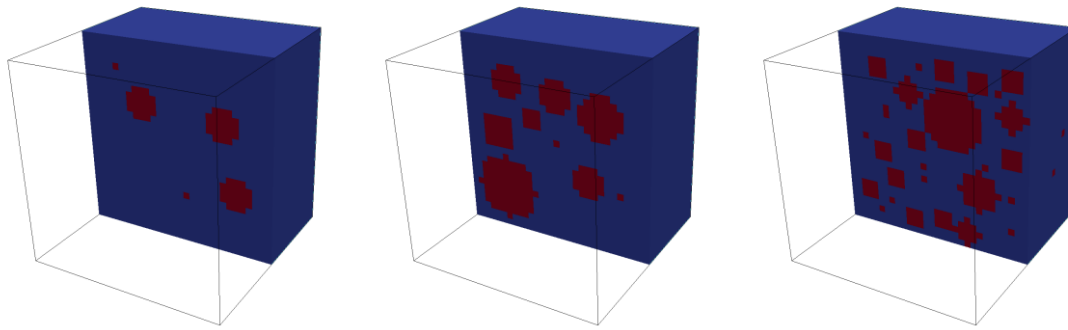
## 222        **3. Parametric studies**

### 223        **3.1.1. Material scale**

224        In this section, physical and numerical parameters related to addition of PCM microcapsules are  
225        assessed on the meso-scale. In order to mimic the experiments, a part of the cement paste was replaced  
226        by PCM microcapsules. For simplicity, the microcapsules are considered to comprise only PCM,  
227        without a hard shell. This was done in order to minimize the computational effort, since in that case a  
228        much finer lattice mesh would need to be used. It is noted that an explicit consideration of a shell  
229        around the microcapsules would have a two-fold influence on the simulation result [49]: (1) it would  
230        reduce the total amount of PCM in the matrix (i.e. part of the capsule would be a non-phase change  
231        material); and (2) it would change the thermal properties of the matrix (due to different density, heat  
232        conductivity, and specific heat capacity of the shell material compared to the matrix). Nevertheless,  
233        the conclusions from the presented analyses are (in a qualitative sense) also valid for the “real” case.

234        In the following simulations it has been assumed that a part of the cement paste has been replaced by  
235        PCM microcapsules. Material properties used in the simulations are given in Table 1. Three  
236        replacement levels are considered: 10%, 20%, and 30% by volume of the cement paste. These  
237        replacement levels are realistic and in line with the work of Fernandes et al. [19]. For all the  
238        simulations in this section, the heat production rate presented in Figure 4 (obtained by De Schutter and  
239        Taerwe [50]), was used. Adiabatic heat evolution is also considered in this section, with all zero flux  
240        boundaries. Initial temperature was set to 20°C (293.15K).

241        In the work of Thiele et al. [31] it was shown that the packing arrangement and polydispersity has no  
242        effect on the effective thermal properties of a composite material containing spherical particles.  
243        Therefore, in this study, three material structures with randomly distributed spherical microcapsules  
244        were created, for the 10%, 20%, and 30% replacement levels, respectively (Figure 6). These material  
245        structures were first voxelized and then overlapped on a lattice mesh (see Figure 2), creating a 2-phase  
246        composite lattice comprising PCM microcapsules and the cement paste.



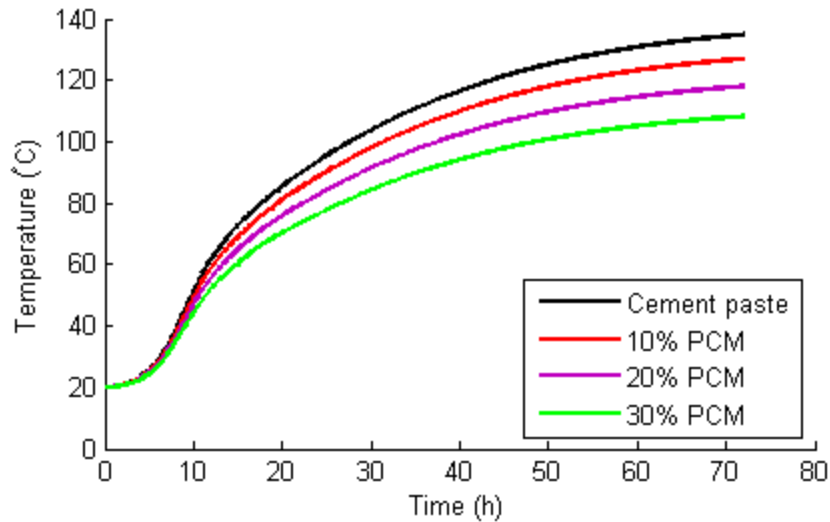
247

248 **Figure 6.**  $30 \times 30 \times 30 \mu\text{m}^3$  material structures comprising PCM microcapsules (cut in the middle to show PCM microcapsules)  
249 and cement paste with (left to right) 10%, 20%, and 30% PCM microcapsules per volume. PCM microcapsules are shown in  
250 red, while blue represents the cement paste matrix.

251 Because the heat production occurs only in the cement paste, the heat source term  $\dot{Q}$  is applied only in  
252 the paste nodes. The phase change capsules have, therefore, a two-fold effect on the internal heat  
253 generation in the composite: first, they have a diluting effect due to the fact that they replace a part of  
254 the hydrating cement; and second, the phase change effect.

255 The diluting effect is considered first. This means that the heat absorbed by the system is only due to  
256 the sensible heat contribution. This essentially means that the PCM is considered simply as a filler  
257 material (e.g. limestone powder or fine sand) in terms of its thermal properties. It is simulated by  
258 considering the specific heat capacity of the PCM microcapsules to be constant (equation (7)).  
259 Temperature evolution for the three simulated PCM replacement levels (together with the reference  
260 cement paste) is given in Figure 7.

261

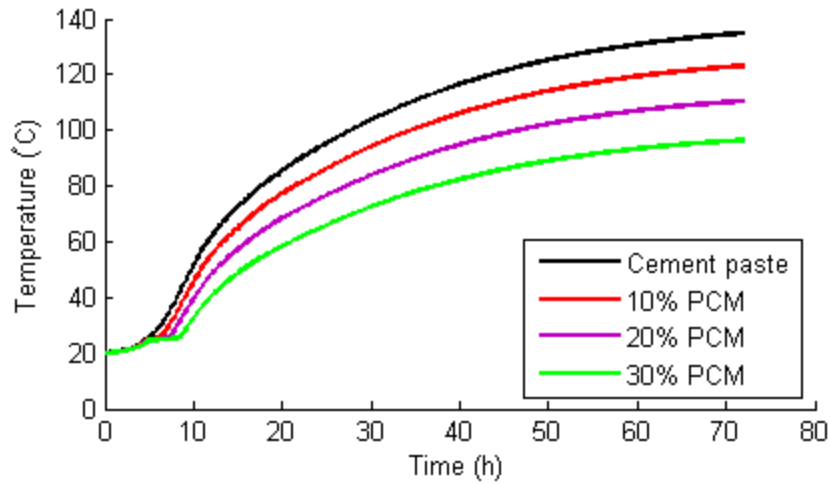


262

263 **Figure 7.** Simulated temperature evolution in a  $30 \times 30 \times 30 \mu\text{m}^3$  microstructure containing different amounts of PCM  
 264 microcapsules and without considering their latent heat contribution.

265 The diluting effect itself can be quite beneficial for the internal heat development, and is actually the  
 266 only mechanism for cases when the initial temperature is higher than the phase change temperature. In  
 267 the simulated example, the temperature achieved after 72 hours (3 days) of hydration was 134.8 °C,  
 268 127 °C, 118 °C, and 108.2 °C for the reference and 10%, 20%, and 30% PCM cases, respectively. This  
 269 means that, by sensible heat only, the temperature can be reduced up to 26°C after three days in  
 270 adiabatic test. It can be also noted that, in this case, the onset of temperature increase is not delayed: it  
 271 is merely reduced due to less hydrating cement in the matrix. This is in accordance with semi-adiabatic  
 272 tests performed by Thiele et al. [32]: they observed that, when the casting temperature was above the  
 273 phase change temperature of the microcapsules (i.e. when only the sensible heat contribution of the  
 274 PCM microcapsules is utilized), only a reduction in peak temperature resulted. The rate of temperature  
 275 rise, however, remained similar.

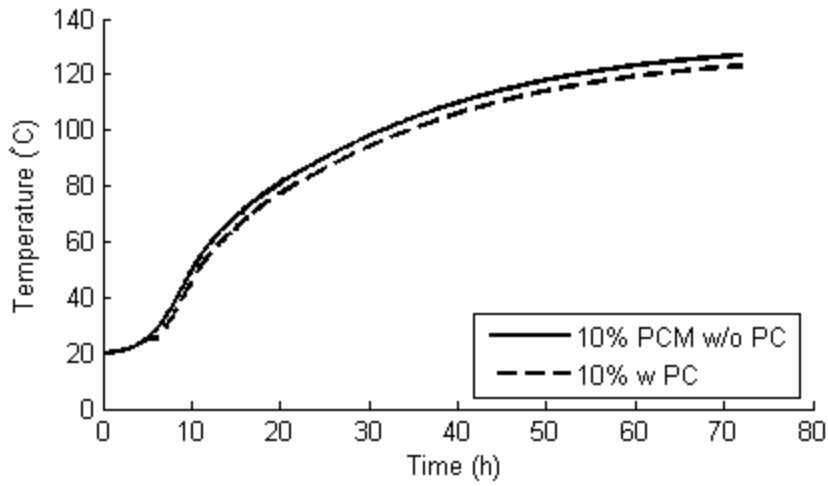
276 Next, the latent heat contribution of the PCM microcapsules is also included. The phase change  
 277 temperature is set as  $T_{pc}=25^\circ\text{C}$ , the latent heat of fusion  $h_f=180 \text{ kJ/kg}$ , and the temperature window as  
 278  $\Delta T_{pc}=3^\circ\text{C}$ . Temperature evolutions for the simulated meso-structures are shown in Figure 8.



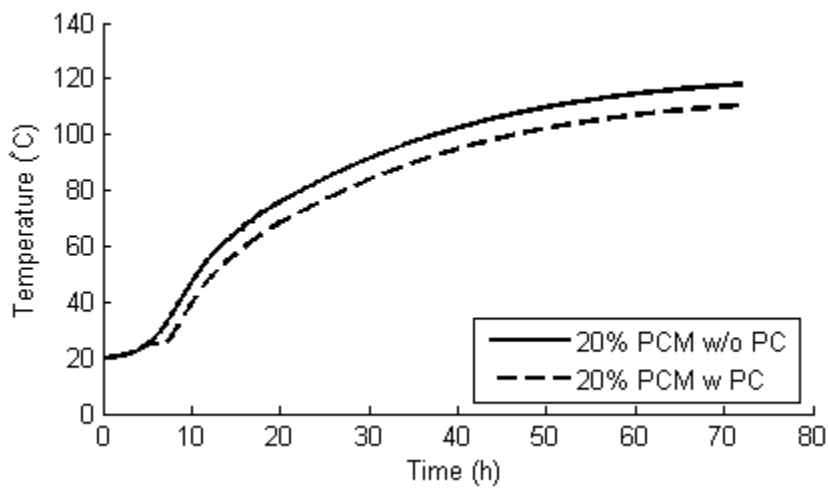
279

280 **Figure 8.** Simulated temperature evolution in a  $30 \times 30 \times 30 \mu\text{m}^3$  microstructure containing different amounts of PCM  
 281 microcapsules.

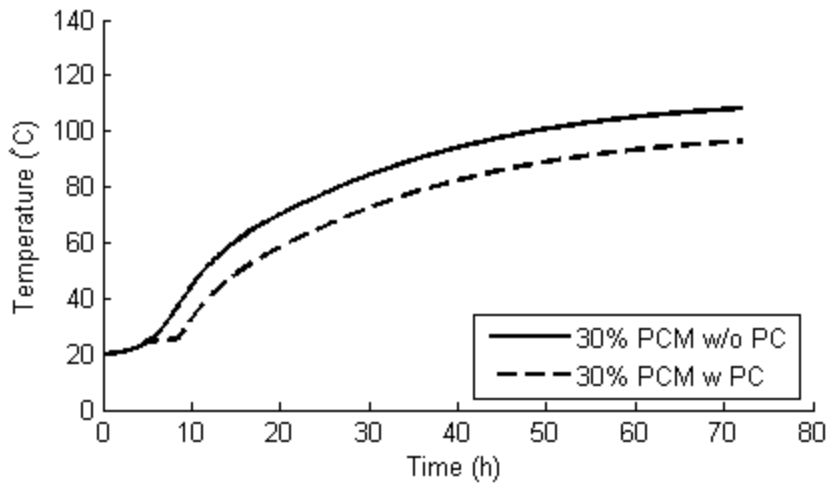
282 It can be seen that the phase-change capsules clearly delay the onset of temperature rise. The  
 283 temperatures achieved after 72 hours are even lower in this case (compared to the case when only the  
 284 sensible heat of PCM microcapsules is considered): 123.1 °C, 110.4 °C, and 96.4 °C. Figure 9 shows  
 285 the latent heat contribution for all considered cases. Figure 10 illustrates the relation between the  
 286 addition of microencapsulated PCMs and the adiabatic temperature rise.



287

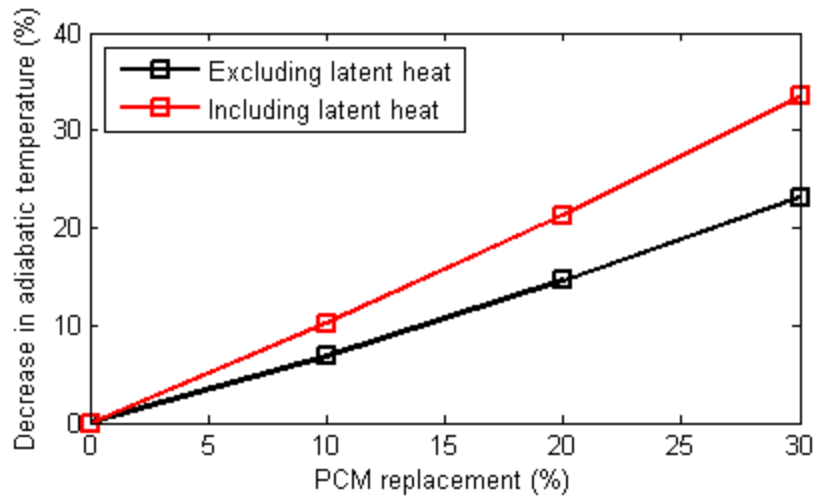


288



289

290 **Figure 9.** Influence of the latent heat contribution of PCM on the adiabatic temperature rise in cement paste containing  
 291 different replacement levels of PCM microcapsules (w/o PC- without phase change, i.e. only diluting effect is considered; w  
 292 PC- phase change, also phase change effect is considered).



293

294

**Figure 10.** Decrease in simulated adiabatic temperature rise after 3 days of hydration with PCM microcapsules.

295

Clearly, the more PCM capsules there are, the more could be gained from their phase change in terms

296

of delaying the temperature rise. The same trend was predicted by theoretical considerations of Qian et

297

al. [18].

298

The ability of PCM microcapsules to absorb heat is highly dependent on their latent heat of fusion.

299

Phase change materials with different latent heat of fusion ( $h_f$ ) are available on the market [21]. In

300

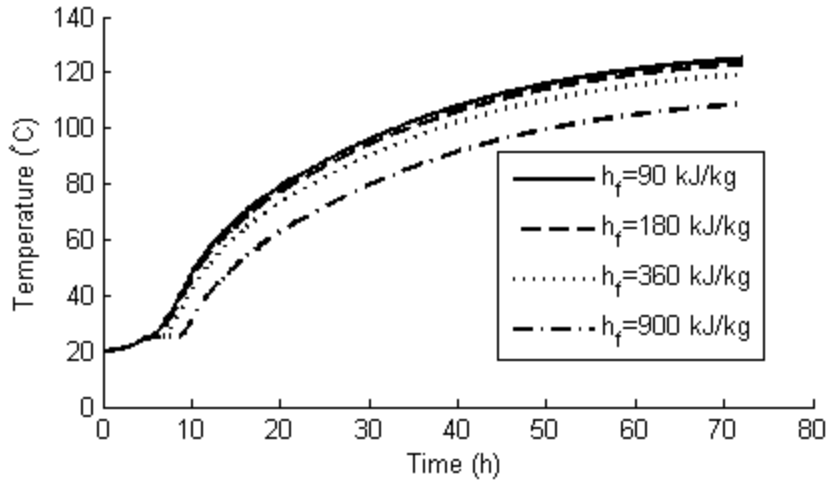
Figure 11, the influence of  $h_f$  on the adiabatic heat evolution for different replacement levels is

301

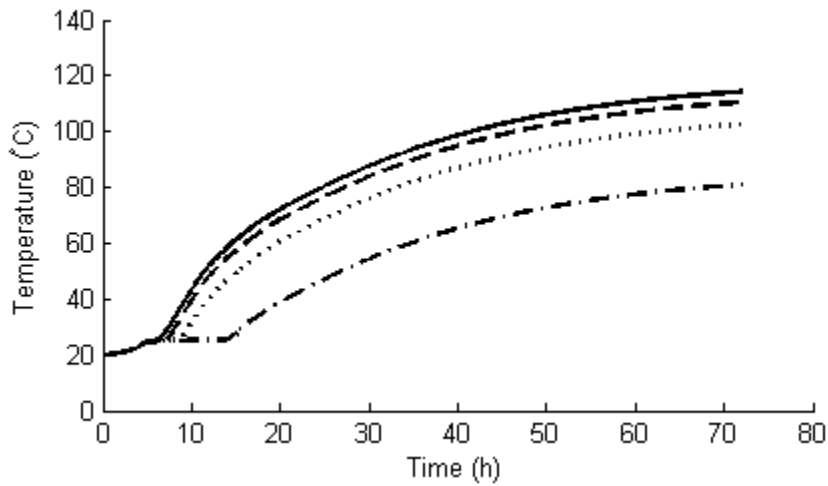
explored. Note that most PCM materials proposed for temperature control in cementitious materials

302

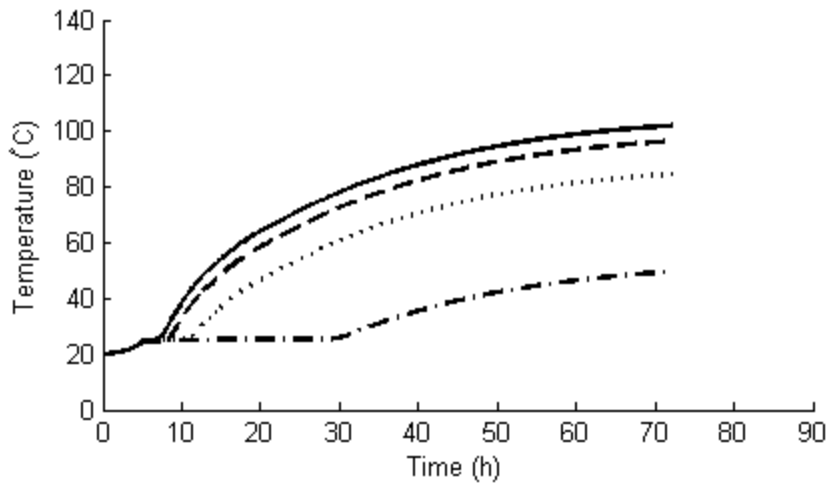
have  $h_f$  between 100-300 kJ/kg [17-19, 27, 49].



303



304



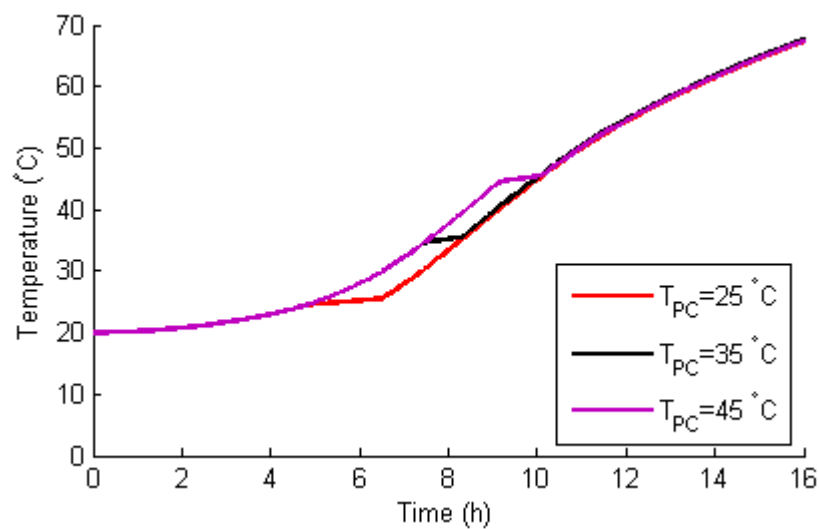
305

306 **Figure 11.** Influence of the latent heat of fusion of PCM microcapsules on the adiabatic temperature rise in cement paste  
 307 containing different replacement levels (top to bottom: 10%, 20%, and 30% PCM microcapsules per volume).

308 In Figure 11 it can be seen that an increase in latent heat of fusion certainly has a great effect on the  
 309 temperature development in adiabatic conditions. It needs to be observed that this increase becomes  
 310 more beneficial as the total amount of PCM in the matrix increases. Therefore, a trade-off is possible

311 between the amount of PCM and their latent heat capacity: lower amounts of PCMs with higher heat  
312 capacity can be used and vice versa, while the temperature development remains similar. However, it  
313 is desirable to use as low amount of PCM microcapsules as possible, since they could have a negative  
314 effect on the compressive [19, 29] and (to a lesser extent) tensile strength of concrete [19].

315 Another important aspect of using PCM microcapsules for control of thermal cracking is their phase  
316 change temperature. In Figure 12, a comparison of systems with three different phase change  
317 temperatures: 25°C, 35°C, and 45°C (with 10% PCM microcapsules and  $h_f=180\text{kJ/kg}$ ).



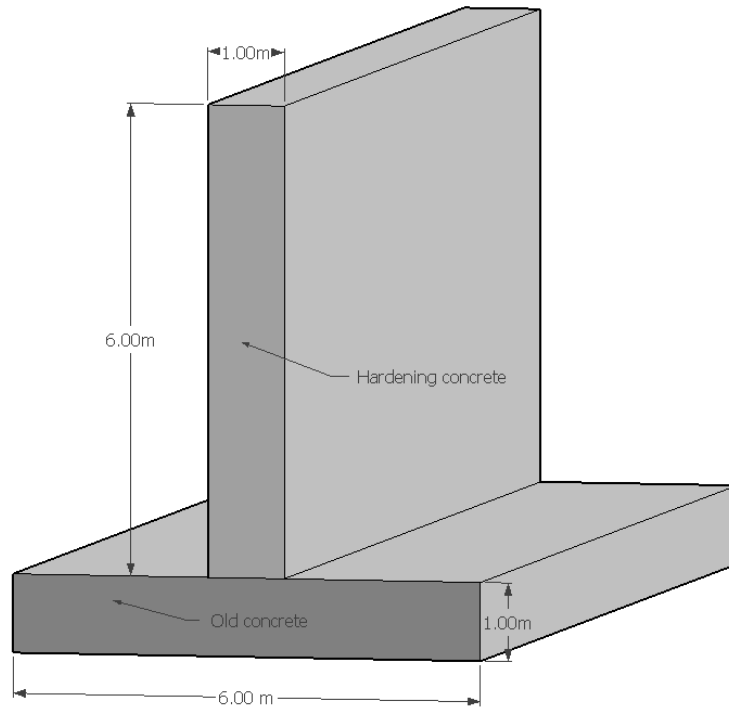
318

319 **Figure 12.** Influence of the phase change temperature of PCM microcapsules on the adiabatic temperature rise in cement  
320 paste containing different replacement levels.

321 It can be seen that the phase change temperature does not affect the final temperature in adiabatic  
322 conditions. In semi-adiabatic conditions (i.e. when some of the heat is lost to the environment), this  
323 may be somewhat different, as explored in the following section.

### 324 3.1.2. Structural scale

325 In this section, the influence of PCM microcapsule addition on temperature and stress development in  
326 hardening concrete wall is explored. As an example, a massive wall-slab system shown in Figure 13 is  
327 analysed. It is assumed in the analysis that the base slab has already hardened, and is restraining the  
328 thermal deformation occurring in the hardening wall. This is a typical scenario which could potentially  
329 lead to through cracking in the concrete wall.



330

331

**Figure 13.** Geometry of the wall-slab system analysed in this section.

332

It is assumed further that the initial temperature of the base slab is 15°C, while the initial temperature

333

of the young concrete is 20°C. The structure is exposed to the constant environmental temperature of

334

15°C. To simulate the heat exchange between the structure and the environment, convective boundary

335

conditions are applied:

$$\overline{q}_B = a(T - T_e)_B \quad (11)$$

336

where  $\overline{q}_B$  is the heat flux normal to the boundary  $B$ ,  $a$  the heat transfer coefficient, and  $T_e$  the

337

temperature of the environment. For all simulations in this section, heat of hydration as shown in

338

Figure 14 is used.

339

Convective boundary conditions are applied on all surfaces of the structure. The hardening concrete is

340

covered by 18mm plywood plate formwork. Wind speed is assumed to be 5 m/s, which together with

341

the formwork results in a heat transfer coefficient of 7 W/m<sup>2</sup>K. Meanwhile, the base slab is directly

342

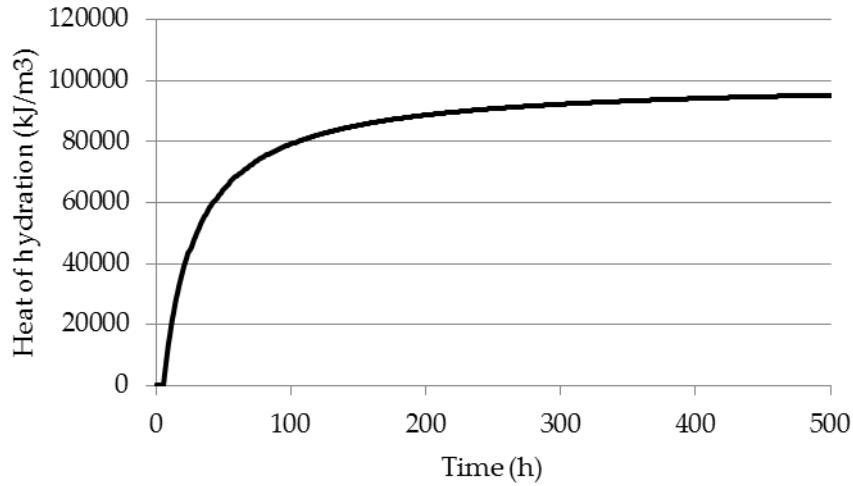
exposed to the wind, resulting in a heat transfer coefficient of 25 W/m<sup>2</sup>K. The formwork is removed

343

after 4 days, and the whole structure is then directly exposed to the environment, with a heat transfer

344

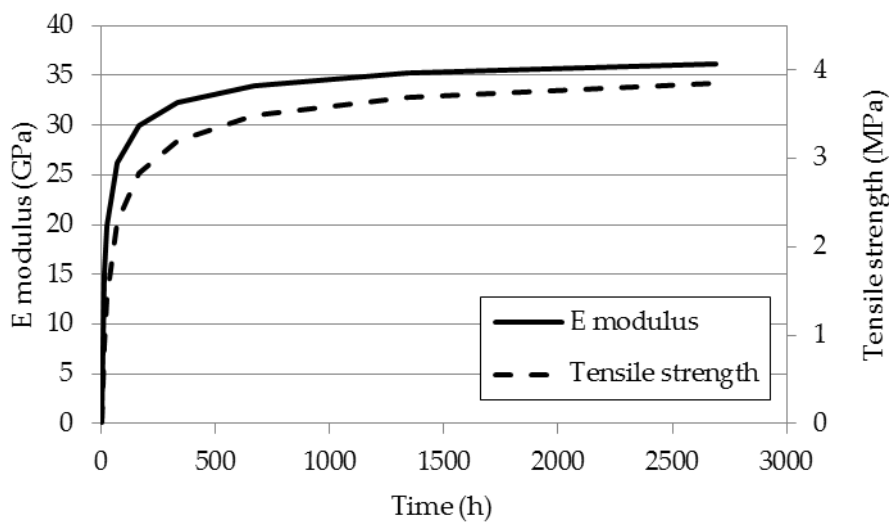
coefficient of 25 W/m<sup>2</sup>K.



345

346 **Figure 14.** Development of heat of hydration of hardening concrete used in macro-scale simulations.

347 Two-dimensional simulations of the wall-slab system are performed, using the plane strain theory  
 348 which is applicable since the out-of-plane dimension (i.e. length) is much larger than the cross-section  
 349 of the structure. Mechanical properties of the hardening concrete are maturity dependent, as given in  
 350 Figure 15. Other properties used in the analyses are given in Table 2. Note that influence of PCM  
 351 microcapsules on mechanical properties of concrete and their development has been neglected in the  
 352 present simulations: although it is known that the PCM microcapsules cause a reduction in the  
 353 compressive strength of concrete [29], they affect the elastic modulus and the tensile/bending strength  
 354 to a lesser extent [19]. These effects will be considered in the model once more data is available.



355

356 **Figure 15.** Development of E modulus and tensile strength of hardening concrete used in macro-scale simulations.

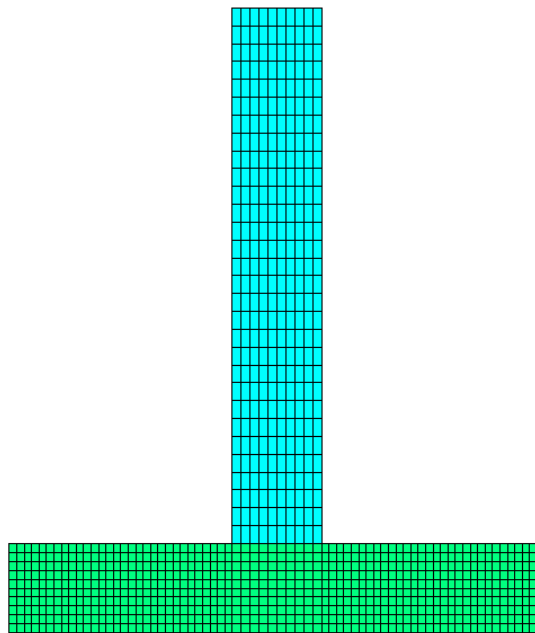
357 **Table 2.** Material properties used in macro-scale simulations.

	Material property	Value
Hardening concrete (wall)	Compressive strength at 28 days	43 MPa
	Tensile strength at 28 days	3.50
	Young's modulus at 28 days	34 Gpa
	Poisson's ratio	0.2
	Coefficient of thermal expansion	$1 \cdot 10^{-5}$ 1/°C
	Density	2300 kg/m <sup>3</sup> , ref. [49]
	Thermal conductivity	1.4 W/mK, ref. [49]
Old concrete (slab)	Specific heat capacity	880 kJ/kgK, ref. [49]
	Thermal conductivity	2.4 W/mK
	Specific heat capacity	1000 kJ/kgK

358

359 The wall/slab system is discretized using fully integrated four node finite elements using the plane  
 360 strain formulation [56]. In total, 1000 elements and 1111 nodes were used in all analyses (Figure 16).

361 The analyses were carried out for 500 hours with a time step of 0.25 hours and storage of the results at  
 362 every 0.5 hours. Time dependent behaviour of concrete (creep and shrinkage) were not considered.

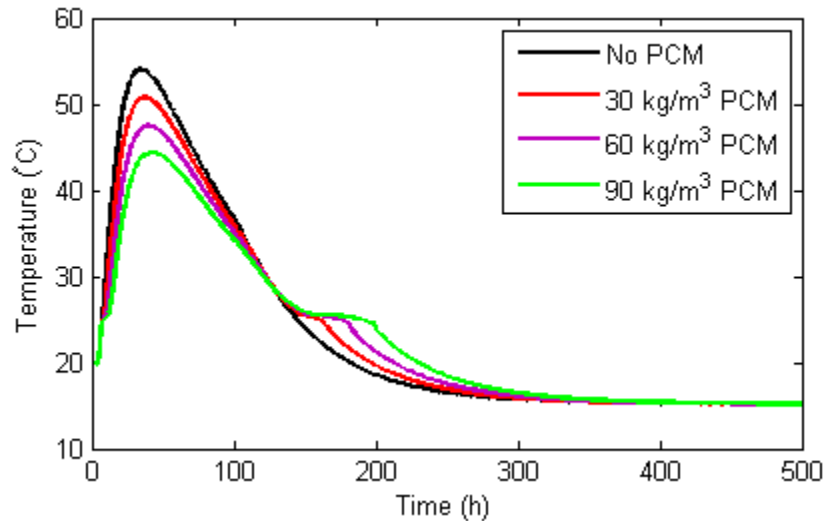


363

364 **Figure 16.** Two dimensional finite element mesh used for simulations in this section. Hardening concrete is shown as light  
 365 blue, while the base slab is shown as green.

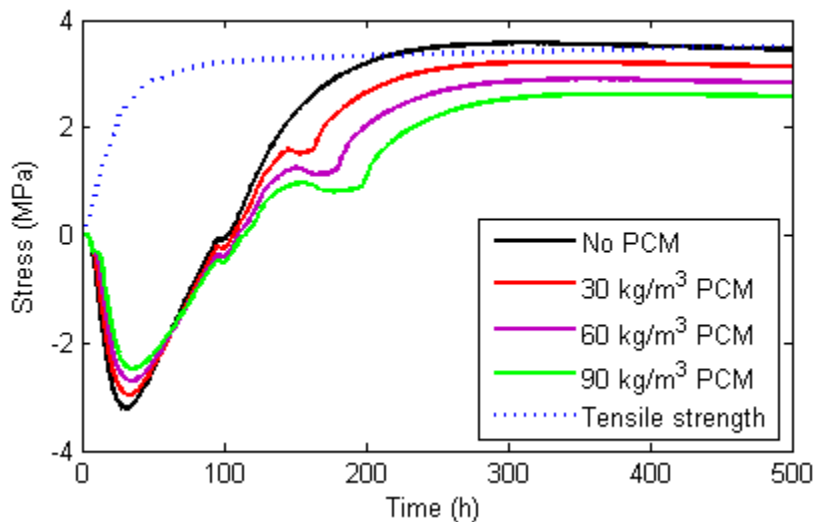
366 First, the influence of PCM microcapsule addition on temperature and stress development in hardening  
 367 concrete is simulated. Four different addition levels are simulated: 0, 30, 60, and 90 kg/m<sup>3</sup> of  
 368 microencapsulated PCM. Note that these addition levels are realistic and in line with existing  
 369 literature: for lightweight aggregates impregnated with PCM, addition levels of 50-120 kg/m<sup>3</sup> have  
 370 been suggested by Sakulich and Bentz [27] as optimum and maximum quantity of PCM in concrete,

371 respectively, while Farnam et al. [26] used even higher quantities ( $150 \text{ kg/m}^3$ ); for microencapsulated  
 372 PCM in concrete, Hunger et al. [29] used  $23\text{-}113 \text{ kg/m}^3$ . In these simulations,  $h_f=180 \text{ kJ/kg}$  [49] and  
 373 phase change temperature of  $25^\circ\text{C}$  are used. Development of maximum temperature and out-of-plane  
 374 stress for these simulations is shown in Figure 17 and Figure 18.



375

376 **Figure 17.** Simulated development of maximum temperature in a hardening concrete wall depending on the PCM  
 377 microcapsule addition level.



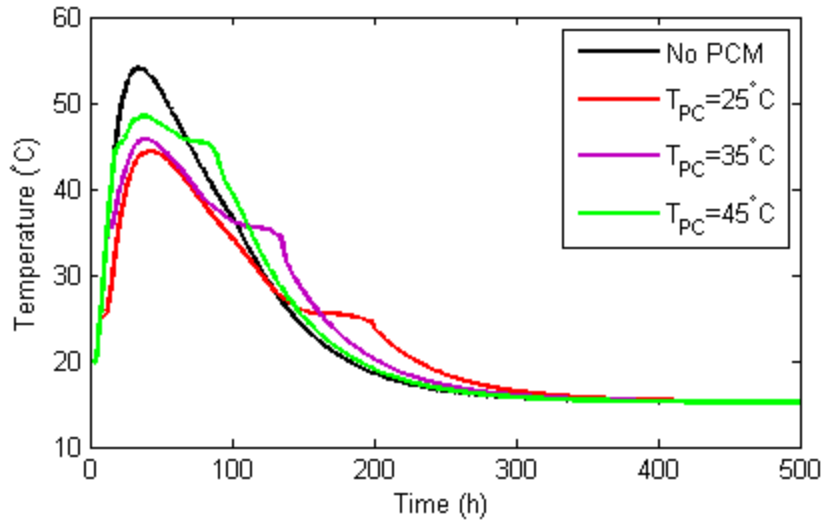
378

379 **Figure 18.** Simulated development of out-of-plane stress in a hardening concrete wall depending on the PCM microcapsule  
 380 addition level.

381 In Figure 17, it can be seen that, as already shown by the meso-scale model (section 3.1.1), the PCM  
 382 microcapsule addition delays the onset of temperature rise. Combined with loss of heat to the  
 383 environment, this results in a lower maximum temperature with increasing PCM addition level.  
 384 Furthermore, the onset of maximum temperature is delayed (Table 3). It is also important that PCM

385 addition slows down the cooling phase, with increasing PCM levels resulting in a smoother  
386 temperature curve. This has implications on the stress development in the hardening wall, as shown in  
387 Figure 18. First, the temperature increase results in occurrence of compressive stresses. The magnitude  
388 of these stresses decreases with the increase in PCM content. However, this phase is not critical for  
389 crack development in the hardening wall: it is the cooling down phase that results in tensile stresses. In  
390 this phase, the PCM addition results in a decrease of tensile stresses in the wall. By comparing the  
391 tensile stresses with the tensile strength of the concrete, it is clear that, when no measures are taken,  
392 cracking will occur. Already when  $30 \text{ kg/m}^3$  of PCM is used, the stresses are lower than the tensile  
393 strength. These stresses also occur at a later instance compared to the reference case  
394 (Table 3). Further increase in PCM content causes an even larger drop in tensile stress. There are two  
395 additional points that need to be stressed again here: on the one hand, the influence of PCM addition  
396 on the tensile strength is not taken into account, and it may be the case that the actual tensile strength  
397 of the PCM concrete is somewhat lower; on the other hand, the influence of PCM on thermal  
398 properties and the dilution effect (section 3.1.1) is also not taken into account, which may result in  
399 even lower stresses. Therefore, these two opposing effects may to a certain extent affect the results.

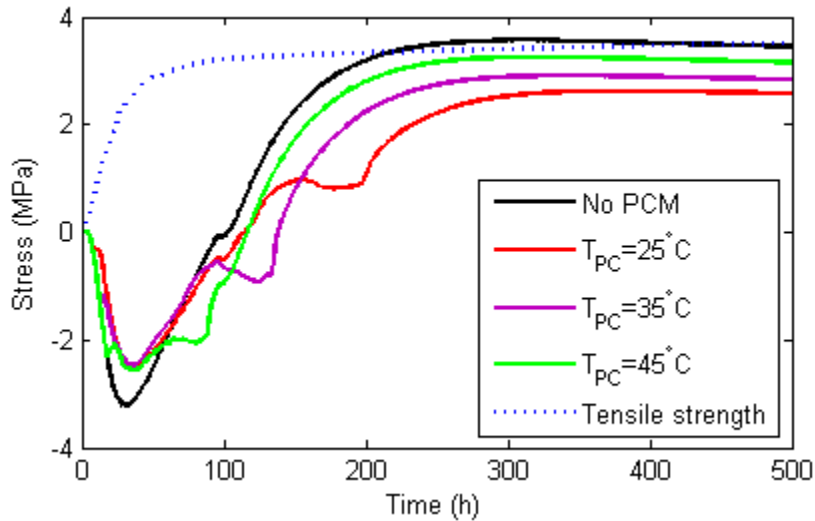
400 Next, the influence of phase change temperature of PCM microcapsules is explored. In section 3.1.1, it  
401 was shown that the temperature of phase change does not have any influence on the maximum  
402 temperature occurring in an adiabatic test. In the structural test, however, part of the heat is lost to the  
403 environment, and the influence of phase change temperature is possibly different. In these simulations,  
404  $h_f=180 \text{ kJ/kg}$  [40] and  $90 \text{ kg/m}^3$  of PCM is assumed. Development of maximum temperature and out-  
405 of-plane stress for these simulations is shown in Figure 19 and Figure 20.



406

407  
408

**Figure 19.** Simulated development of maximum temperature in a hardening concrete wall depending on the phase change temperature of PCM microcapsules.



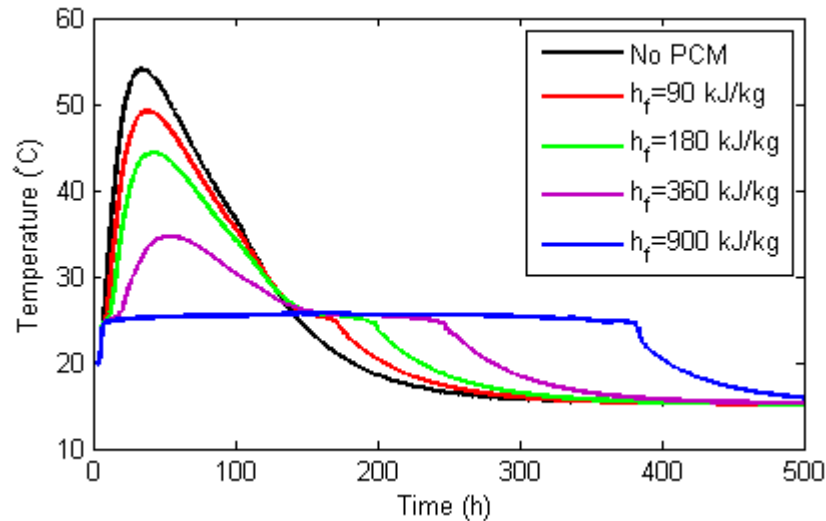
409

410  
411

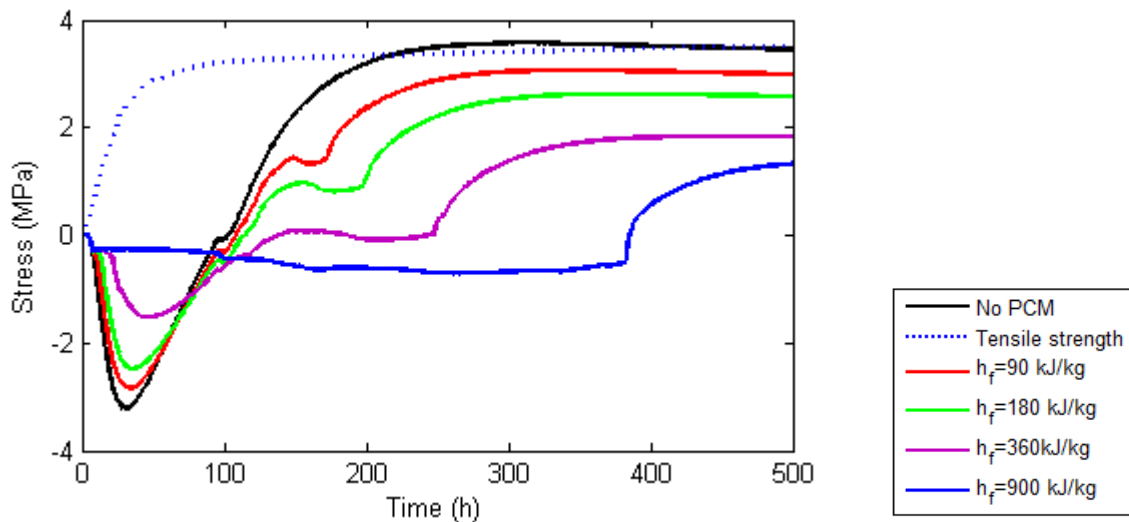
**Figure 20.** Simulated development of out-of-plane stress in a hardening concrete wall depending on the phase change temperature of PCM microcapsules.

412 Three different phase change temperatures are explored: 25°C, 35°C, and 45°C. It can be seen in  
 413 Figure 19 that lower PCM temperatures result in lower maximum temperature (for the assumed  
 414 casting temperature of 20°C and the assumed material and environmental parameters). The cooling-  
 415 down phase shows a similar behaviour: the highest phase change temperature prolongs the cooling  
 416 down phase less than the lowest phase change temperature. This results in marked differences in  
 417 maximum tensile stress that occurs in this phase: for the lowest phase change temperature, lowest  
 418 stresses occur and at the later stage (Figure 20 and Table 3). This will result in a lower probability of  
 419 thermal cracking.

420 Finally, the influence of heat of fusion of PCM microcapsules is explored. Similar to the meso-scale  
 421 model in section 3.1.1., heats of fusion ranging from 90-900 kJ/kg were explored. In this set of  
 422 simulations, 90 kg/m<sup>3</sup> of PCM was assumed with a phase change temperature of 25°C. Development  
 423 of maximum temperature and out-of-plane stress for these simulations is shown in figures 21 and 22.



424  
 425 **Figure 21.** Simulated development of maximum temperature in a hardening concrete wall depending on the heat of fusion of  
 426 PCM microcapsules.



427  
 428 **Figure 22.** Simulated development of out-of-plane stress in a hardening concrete wall depending on the heat of fusion of  
 429 PCM microcapsules.

430 As expected and in accordance with the meso-scale model, the increase in heat of fusion of PCM  
 431 microcapsules causes a decrease in maximum temperature (Figure 21). Furthermore, it prolongs the  
 432 cooling phase. In the extreme case of  $h_f=900$  kJ/kg (which is probably not feasible in practice), there is  
 433 hardly any increase in temperature (about 5°C, Table 3). Tensile stresses occurring in the cooling

434 down phase decrease with the increase in heat of fusion (Figure 22). It needs to emphasized again here  
 435 that a trade-off between the heat of fusion and quantity of PCM microcapsules is possible, and that use  
 436 of a smaller quantity of PCM microcapsules with high heat of fusion is desirable in order to minimize  
 437 the loss of mechanical properties.

438 **Table 3.** Summary of the macro-scale simulation results.

In common	Analysis	Max temperature (°C)	Occurring at (h)	Max stress (MPa)	Occurring at (h)
$T_{pc}=25^{\circ}\text{C}$ , $h_f=180\text{ kJ/kg}$	No PCM	54	34.5	3.56	302
	30 kg/m <sup>3</sup>	50.76	37	3.21	331.5
	60 kg/m <sup>3</sup>	47.47	39.5	2.89	347
	90 kg/m <sup>3</sup>	44.34	42	2.62	372
$90\text{ kg/m}^3$ , $h_f=180\text{ kJ/kg}$	$T_{pc}=35^{\circ}\text{C}$	45.77	38.5	2.91	334.5
	$T_{pc}=45^{\circ}\text{C}$	48.46	38.5	3.25	315
$90\text{ kg/m}^3$ , $T_{pc}=25^{\circ}\text{C}$	$h_f=90\text{ kJ/kg}$	49.17	38.5	3.06	339
	$h_f=360\text{ kJ/kg}$	34.68	54	1.83	434.5
	$h_f=900\text{ kJ/kg}$	25.75	164	1.32	500

439  
 440 It should be stressed that the quantitative findings of the presented analyses are limited by the  
 441 assumptions adopted. For example, if the environment would be warmer, it is possible that the optimal  
 442 temperature of phase change would be different than the one found for the considered conditions.  
 443 Furthermore, it is possible that, in certain cases, it would be desirable to combine the use of PCM  
 444 microcapsule addition with traditional measures for control of thermal cracking, such as decrease of  
 445 casting temperature through use of ice [54]. The model presented is versatile and different input  
 446 parameters and measures can be considered and combined. In the future, the model will be applied for  
 447 simulating large-scale experiments related to control of temperature rise and thermal cracking through  
 448 use of PCM microcapsules.

#### 449 **4. General discussion**

450 Simulations considering the material on the meso-scale (section 3.1.1) have revealed several  
 451 important aspects related to use of microencapsulated phase change materials to reduce temperature  
 452 rise in cement paste. PCM microcapsules reduce the temperature through a synergy of two  
 453 mechanisms: the dilution effect and the capture of heat through phase change. It should be noted that  
 454 the former does not delay the onset of temperature rise, while the latter does. It was also shown that he

455 higher the amount of PCM microcapsules, the longer the temperature rise will be delayed. The same  
456 goes for the latent heat of fusion: the higher the latent heat of fusion of PCM microcapsules, the later  
457 the temperature rise will occur. It can be inferred that a trade-off between these two factors is possible.  
458 Note that use of a lower amount of PCM microcapsules with high latent heat of fusion is beneficial  
459 from a structural point of view, since the decrease of (compressive) strength has shown to be  
460 proportional to the PCM addition in cement paste [19], although this is not always the case for mortar  
461 and concrete [57]. Finally, it was shown that the phase change temperature ( $T_{PC}$ ) does not influence  
462 the adiabatic temperature rise. This means that, depending on the environmental conditions expected,  
463 the phase change temperature of microencapsulated PCMs can be tailored without affecting the  
464 maximum (theoretical) temperature which may occur.

465 Full-scale (structural) simulations (section 3.1.2) have focused on the interaction between the  
466 hardening concrete structure, external restraints, and the environment. Building up on the meso-scale  
467 analysis, the aim of this section was to prove that the decrease in temperature rise due to addition of  
468 microencapsulated PCMs can reduce the maximum tensile stress occurring in the structure. It was  
469 shown by the simulations to be possible, even for relatively low amounts of considered PCM  
470 microcapsules ( $30\text{kg/m}^3$ ). The main contribution to stress reduction seems not to come from the  
471 reduced peak temperature, but from the prolonged period of cooling down compared to the case when  
472 no PCMs are added to the mix. This means that the temperature difference between different parts of  
473 the structure are lowered, leading to lower stresses. In addition, the occurrence of maximum tensile  
474 stress is delayed in proportion to the PCM addition (or the latent heat of fusion), meaning that the time  
475 dependent mechanical properties (most pertinent being the tensile strength in this case) will be higher,  
476 thereby further reducing the risk of cracking. Furthermore, full-scale simulations showed a significant  
477 influence of the phase change temperature ( $T_{PC}$ ) on temperature and stress development. This means  
478 that PCMs need to be tailored for expected environmental conditions.

479 Several important aspects have been neglected in the present work for simplicity. In meso-scale  
480 simulations, the existence of a hard shell around PCM was neglected, and the microcapsules were  
481 considered to comprise pure phase change material. The existence of a (polymeric) hard shell would,

482 to a certain extent, influence the thermal properties of the considered composite. Furthermore, it would  
483 reduce the effective amount of the PCM (for a given microcapsule volume) and thus the total heat  
484 storage capacity. In full-scale simulations, also, it was assumed that the PCM addition does not affect  
485 the density, thermal conductivity, or the specific heat capacity of concrete. This may, to a certain  
486 extent, affect the temperature distribution in the considered structure. Probably the most important  
487 simplification in the full-scale model was neglecting the influence of the PCM microcapsule addition  
488 on the mechanical properties of concrete. Although it was found that addition of a significant  
489 percentage of PCM can have a negative effect on compressive and tensile strength [19, 29, 58], the  
490 fracture toughness remains largely intact [19]. Furthermore, the addition of compliant inclusions may  
491 increase the creep and relaxation of the hardening concrete [59], thereby reducing the stresses.  
492 Finally, it was implicitly assumed that the all PCM microcapsules added to the mix will survive the  
493 mixing process and remain intact. However, it is possible that some PCM microcapsules break during  
494 the mixing of the concrete [19, 58]. If this would happen, it is possible that chemical reactions between  
495 the PCM and the hydration products would occur. For example, Farnam et al. [26] found that methyl  
496 laureate reacts with the cementitious matrix causing an expansive reaction and cracking of the mortar.  
497 All these aspects will be considered in the future when more experimental data is available.

## 498 **5. Summary and conclusions**

499 In this work, the influence of phase change materials (PCMs) addition (in the form of microcapsules)  
500 on hydration temperature evolution and stress development in hardening concrete is studied using  
501 numerical models. First, addition of discrete microcapsules is considered on the meso-scale (i.e.  
502 cement paste level) using the lattice model. The influence of PCM percentage, phase change  
503 temperature, and latent heat of fusion on the adiabatic temperature development is studied on this  
504 scale. Meso-scale simulations have revealed the following:

- 505 • The addition of PCM microcapsules in cement paste reduces the adiabatic heat rise through  
506 two mechanisms. First, the sensible heat contribution (together with the diluting effect) can  
507 reduce the total heat rise, without affecting the onset of the temperature rise. Second, the latent  
508 heat contribution will delay the onset of temperature rise.

- 509       • The latent heat contribution becomes more dominant as the percentage of PCM microcapsules  
510       increases. This can be exploited by increasing the latent heat of fusion of the PCM  
511       microcapsules.
- 512       • The phase change temperature of PCM microcapsules does not affect the heat rise in an  
513       *adiabatic* test.

514   Additionally, a commercial FE package is used on the macro-scale (i.e. concrete level) to study the  
515   behaviour of a structural system comprising a hardening wall on a slab. The influence of PCM  
516   addition, phase change temperature, and latent heat of fusion on the semi-adiabatic temperature rise  
517   and stress development in the hardening wall is explored. Based on the structural-scale analyses, the  
518   following conclusions can be drawn:

- 519       • In *semi-adiabatic* (i.e. field) conditions, the addition of PCM in hardening concrete has  
520       potential to delay the temperature rise, reduce the maximum tensile stress, and delay its  
521       occurrence. The maximum tensile stress is inversely proportional to the amount of PCM added  
522       to the mix.
- 523       • In *semi-adiabatic* conditions, the phase change temperature does influence the maximum  
524       temperature developing in the structure. In the considered example, the lowest phase change  
525       temperature (25°C) resulted in the lowest maximum temperature. Furthermore, it also resulted  
526       in the lowest magnitude of tensile stresses occurring at a later time compared to other  
527       simulated phase change temperatures. Consequently, it has the lowest probability of cracking.  
528       Note that this is related to the environmental conditions, and that the PCMs may need to be  
529       tailored depending on the climate.
- 530       • An increase in the latent heat of fusion serves the same purpose as an increase in PCM  
531       addition: it lowers the maximum temperature and maximum stress, and delays their  
532       occurrence. Especially the cooling phase is prolonged. Therefore, a trade-off between the heat  
533       of fusion and quantity of PCM microcapsules is possible, where a smaller amount of PCMs  
534       with a higher heat of fusion can be used with the same (thermal) efficiency. This would be  
535       beneficial also in terms of mechanical properties of the concrete.

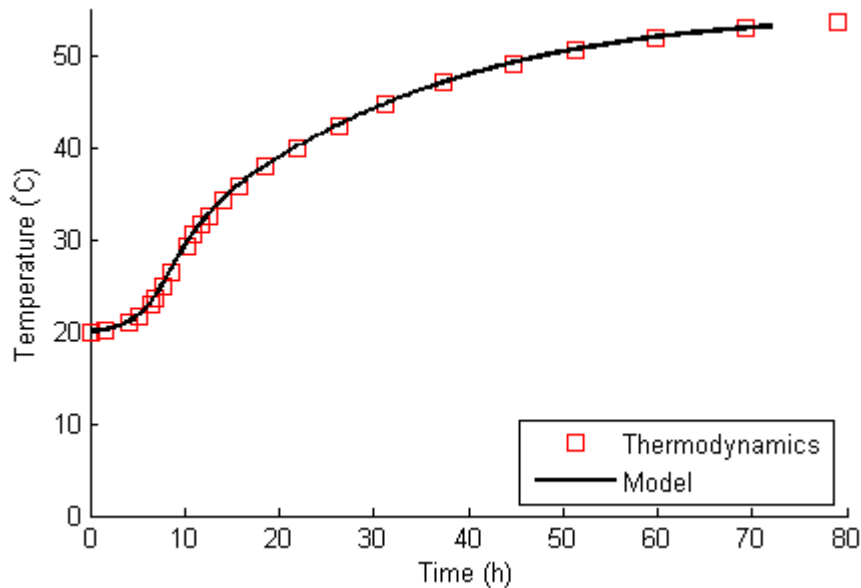
536 The present paper clearly proves that, in theory, properly designed cementitious materials with  
537 incorporated microencapsulated PCMs have potential to reduce heat evolution and thus mitigate early  
538 age thermal cracking. There are numerous issues that need to be addressed before this can be done in  
539 engineering practice. First, proper encapsulation of PCM is essential: microcapsules need to be hard  
540 enough to sustain mixing and pouring of the concrete, and stable in a highly alkaline environment of  
541 concrete for longer periods of time. Second, if it intended that the same microcapsules be used to  
542 reduce thermal fatigue of concrete, it is necessary that the PCM material itself is stable and that it can  
543 sustain numerous solid-to-liquid transitions (and vice versa) without losing its latent heat storing  
544 ability. And third, for structural applications, it is important that these relatively soft and compliant  
545 inclusions do not affect strength, creep, and shrinkage to very high extents. All of these issues need to  
546 be addressed prior to fully recommending the use of microencapsulated PCMs in engineering practice.  
547 This will form a basis of the experimental part of the current research project and will be studied in the  
548 near future.

## 549 **Acknowledgements**

550 The authors would like to acknowledge the financial support by the EU-Infravation (An Infrastructure  
551 Innovation Programme) for the project ECLIPS – Enhancing Concrete Life in Infrastructure Through  
552 Phase-change systems.

## 553 **Appendix**

554 In order to assure that the meso-scale model provides realistic results in terms of adiabatic temperature  
555 rise, here an adiabatic experiment performed on concrete is simulated. The same  $30 \times 30 \times 30 \mu\text{m}^3$   
556 specimen as in section 2.1.2 is used with the heat production rate given in figure 6. The concrete  
557 mixture used by De Schutter and Taerwe is used [50], with  $300 \text{ kg/m}^3$  of cement and unit weight of  
558  $2400 \text{ kg/m}^3$ . The specific heat capacity was set to  $1000 \text{ kJ/kg}$ , and the initial temperature to  $20^\circ\text{C}$ .  
559 Figure 23 gives the theoretical (thermodynamics) temperature rise and that calculated using the meso-  
560 scale model. It can be seen that the model shows a realistic rise of temperature, and that it matches the  
561 thermodynamic calculations quite well.



562

563

**Figure 23.** Comparison of the simulated temperature evolution and thermodynamic calculations for concrete.

564 **References:**

565 [1] Emborg M, Bernander S. Assessment of risk of thermal cracking in hardening concrete. *Journal of*  
566 *Structural Engineering*. 1994;120(10):2893-912.

567 [2] De Schutter G. Finite element simulation of thermal cracking in massive hardening concrete  
568 elements using degree of hydration based material laws. *Computers & Structures*. 2002;80(27):2035-  
569 42.

570 [3] Yuan Y, Wan Z. Prediction of cracking within early-age concrete due to thermal, drying and creep  
571 behavior. *Cement and Concrete Research*. 2002;32(7):1053-9.

572 [4] Mehta PK, Monteiro PJ. *Concrete: microstructure, properties, and materials*: McGraw-Hill New  
573 York; 2006.

574 [5] Waller V, d'Aloia L, Cussigh F, Lecrux S. Using the maturity method in concrete cracking control at  
575 early ages. *Cement and Concrete Composites*. 2004;26(5):589-99.

576 [6] Bolander JE, Kim K, Sasaki K. Thermal effects on early-age cracking potential of concrete bridge  
577 decks. In: Bićanić N, Mang H, Meschke G, de Borst R, editors. *Computational Modelling of Concrete*  
578 *Structures*. St. Anton am Arlberg: CRC Press; 2014. p. 723-9.

579 [7] ACI. *Cement and Concrete Terminology (ACI 116R-00)*. USA: American Concrete Institute Pubs;  
580 2000.

581 [8] Gajda J, Vangeem M. Controlling temperatures in mass concrete. *Concrete international*.  
582 2002;24(1):58-62.

583 [9] Malhotra VM, Ramezani pour A. *Fly ash in concrete*: Canmet; 1994.

584 [10] Atiş CD. Heat evolution of high-volume fly ash concrete. *Cement and Concrete Research*.  
585 2002;32(5):751-6.

586 [11] Šavija B, Schlangen E, Pacheco J, Millar S, Eichler T, Wilsch G. Chloride ingress in cracked  
587 concrete: a laser induced breakdown spectroscopy (LIBS) study. *Journal of Advanced Concrete*  
588 *Technology*. 2014;12(10):425-42.

589 [12] Kwon SJ, Na UJ, Park SS, Jung SH. Service life prediction of concrete wharves with early-aged  
590 crack: Probabilistic approach for chloride diffusion. *Structural Safety*. 2009;31(1):75-83.

591 [13] Blagojević A. *The Influence of Cracks on the Durability and Service Life of Reinforced Concrete*  
592 *Structures in relation to Chloride-Induced Corrosion: A Look from a Different Perspective*: TU Delft,  
593 Delft University of Technology; 2016.

594 [14] Nobuhiro M, Kazuo U. Nonlinear thermal stress analysis of a massive concrete structure.  
595 Computers & Structures. 1987;26(1):287-96.

596 [15] Pane I, Hansen W. Investigation of blended cement hydration by isothermal calorimetry and  
597 thermal analysis. Cement and Concrete Research. 2005;35(6):1155-64.

598 [16] Kim JK, Kim KH, Yang JK. Thermal analysis of hydration heat in concrete structures with pipe-  
599 cooling system. Computers & Structures. 2001;79(2):163-71.

600 [17] Bentz DP, Turpin R. Potential applications of phase change materials in concrete technology.  
601 Cement and Concrete Composites. 2007;29(7):527-32.

602 [18] Qian C, Gao G, Zhu C, Guo Z. Influence of phase change materials on temperature rise caused by  
603 hydration heat evolution of cement-based materials. Magazine of Concrete Research.  
604 2010;62(11):789-94.

605 [19] Fernandes F, Manari S, Aguayo M, Santos K, Oey T, Wei Z, et al. On the feasibility of using phase  
606 change materials (PCMs) to mitigate thermal cracking in cementitious materials. Cement and  
607 Concrete Composites. 2014;51:14-26.

608 [20] Qian C, Gao G. Reduction of interior temperature of mass concrete using suspension of phase  
609 change materials as cooling fluid. Construction and Building Materials. 2012;26(1):527-31.

610 [21] Zalba B, Marín JM, Cabeza LF, Mehling H. Review on thermal energy storage with phase change:  
611 materials, heat transfer analysis and applications. Applied thermal engineering. 2003;23(3):251-83.

612 [22] Hawes D, Banu D, Feldman D. Latent heat storage in concrete. II. Solar energy materials.  
613 1990;21(1):61-80.

614 [23] Lamberg P, Lehtiniemi R, Henell A-M. Numerical and experimental investigation of melting and  
615 freezing processes in phase change material storage. International Journal of Thermal Sciences.  
616 2004;43(3):277-87.

617 [24] Snoeck D, Priem B, Dubruel P, De Belie N. Encapsulated Phase-Change Materials as additives in  
618 cementitious materials to promote thermal comfort in concrete constructions. Materials and  
619 Structures. 2016;49(1):225-39.

620 [25] Ling T-C, Poon C-S. Use of phase change materials for thermal energy storage in concrete: an  
621 overview. Construction and Building Materials. 2013;46:55-62.

622 [26] Farnam Y, Krafcik M, Liston L, Washington T, Erk K, Tao B, et al. Evaluating the Use of Phase  
623 Change Materials in Concrete Pavement to Melt Ice and Snow. Journal of Materials in Civil  
624 Engineering. 2015:04015161.

625 [27] Sakulich AR, Bentz D. Incorporation of phase change materials in cementitious systems via fine  
626 lightweight aggregate. Construction and Building Materials. 2012;35:483-90.

627 [28] Cabeza LF, Castellon C, Nogues M, Medrano M, Leppers R, Zubillaga O. Use of  
628 microencapsulated PCM in concrete walls for energy savings. Energy and Buildings. 2007;39(2):113-9.

629 [29] Hunger M, Entrop A, Mandilaras I, Brouwers H, Founti M. The behavior of self-compacting  
630 concrete containing micro-encapsulated phase change materials. Cement and Concrete Composites.  
631 2009;31(10):731-43.

632 [30] Pasupathy A, Velraj R, Seeniraj R. Phase change material-based building architecture for thermal  
633 management in residential and commercial establishments. Renewable and Sustainable Energy  
634 Reviews. 2008;12(1):39-64.

635 [31] Thiele AM, Kumar A, Sant G, Pilon L. Effective thermal conductivity of three-component  
636 composites containing spherical capsules. International Journal of Heat and Mass Transfer.  
637 2014;73:177-85.

638 [32] Thiele AM, Wei Z, Falzone G, Young BA, Neithalath N, Sant G, et al. Figure of merit for the  
639 thermal performance of cementitious composites containing phase change materials. Cement and  
640 Concrete Composites. 2016;65:214-26.

641 [33] Bolander J, Saito S. Fracture analyses using spring networks with random geometry. Engineering  
642 Fracture Mechanics. 1998;61(5):569-91.

643 [34] Schlangen E, Van Mier J. Simple lattice model for numerical simulation of fracture of concrete  
644 materials and structures. Materials and Structures. 1992;25(9):534-42.

645 [35] Grassl P, Jirásek M. Meso-scale approach to modelling the fracture process zone of concrete  
646 subjected to uniaxial tension. *International Journal of Solids and Structures*. 2010;47(7):957-68.

647 [36] Sands CM. An irregular lattice model to simulate crack paths in bonded granular assemblies.  
648 *Computers & Structures*. 2016;162:91-101.

649 [37] Šavija B, Liu D, Smith G, Hallam KR, Schlangen E, Flewitt PE. Experimentally informed multi-scale  
650 modelling of mechanical properties of quasi-brittle nuclear graphite. *Engineering Fracture*  
651 *Mechanics*. 2016;153:360-77.

652 [38] Liu L, Ye G, Schlangen E, Chen H, Qian Z, Sun W, et al. Modeling of the internal damage of  
653 saturated cement paste due to ice crystallization pressure during freezing. *Cement and Concrete*  
654 *Composites*. 2011;33(5):562-71.

655 [39] Schlangen E, Qian Z. 3D modeling of fracture in cement-based materials. *Journal of Multiscale*  
656 *Modelling*. 2009;1(02):245-61.

657 [40] Yip M, Mohle J, Bolander J. Automated modeling of three-dimensional structural components  
658 using irregular lattices. *Computer-Aided Civil and Infrastructure Engineering*. 2005;20(6):393-407.

659 [41] Bolander JE, Berton S. Simulation of shrinkage induced cracking in cement composite overlays.  
660 *Cement and Concrete Composites*. 2004;26(7):861-71.

661 [42] Luković M, Šavija B, Schlangen E, Ye G, van Breugel K. A 3D Lattice Modelling Study of Drying  
662 Shrinkage Damage in Concrete Repair Systems. *Materials*. 2016;9(7):575.

663 [43] Šavija B, Pacheco J, Schlangen E. Lattice modeling of chloride diffusion in sound and cracked  
664 concrete. *Cement and Concrete Composites*. 2013;42:30-40.

665 [44] Wang L, Ueda T. Mesoscale modelling of the chloride diffusion in cracks and cracked concrete.  
666 *Journal of Advanced Concrete Technology*. 2011;9(3):241-9.

667 [45] Šavija B, Luković M, Schlangen E. Lattice modeling of rapid chloride migration in concrete.  
668 *Cement and Concrete Research*. 2014;61:49-63.

669 [46] Pacheco J, Šavija B, Schlangen E, Polder RB. Assessment of cracks in reinforced concrete by  
670 means of electrical resistance and image analysis. *Construction and Building Materials*. 2014;65:417-  
671 26.

672 [47] Lewis R, Nithiarasu P, Seetharamu K. *Fundamentals of the Finite Element Method for Heat and*  
673 *Fluid Flow*, 2004. John Wiley & Sons; 2004.

674 [48] Nakamura H, Srisoros W, Yashiro R, Kunieda M. Time-dependent structural analysis considering  
675 mass transfer to evaluate deterioration process of RC structures. *Journal of Advanced Concrete*  
676 *Technology*. 2006;4(1):147-58.

677 [49] Thiele AM, Sant G, Pilon L. Diurnal thermal analysis of microencapsulated PCM-concrete  
678 composite walls. *Energy Conversion and Management*. 2015;93:215-27.

679 [50] De Schutter G, Taerwe L. General hydration model for Portland cement and blast furnace slag  
680 cement. *Cement and Concrete Research*. 1995;25(3):593-604.

681 [51] Van Breugel K. Numerical simulation of hydration and microstructural development in hardening  
682 cement-based materials:(II) applications. *Cement and Concrete Research*. 1995;25(3):522-30.

683 [52] Ye G. Experimental study and numerical simulation of the development of the microstructure  
684 and permeability of cementitious materials: TU Delft, Delft University of Technology; 2003.

685 [53] Liwu M, Min D. Thermal behavior of cement matrix with high-volume mineral admixtures at  
686 early hydration age. *Cement and Concrete Research*. 2006;36(10):1992-8.

687 [54] Van Beek A, Baetens B, Schlangen E. Numerical model for prediction of cracks in concrete  
688 structures. PRO 23: International RILEM Conference on Early Age Cracking in Cementitious Systems-  
689 EAC'01: RILEM Publications; 2002. p. 39.

690 [55] Schlangen E. Online help/manual module HEAT of FEMMASSE. The Netherlands. 2000.

691 [56] Zienkiewicz OC, Taylor RL, Taylor RL. *The finite element method*: McGraw-hill London; 1977.

692 [57] Aguayo M, Das S, Maroli A, Kabay N, Mertens JC, Rajan SD, et al. The influence of  
693 microencapsulated phase change material (PCM) characteristics on the microstructure and strength  
694 of cementitious composites: Experiments and finite element simulations. *Cement and Concrete*  
695 *Composites*. 2016;73:29-41.

696 [58] Cunha S, Aguiar J, Ferreira V, Tadeu A. Mortars based in different binders with incorporation of  
697 phase-change materials: Physical and mechanical properties. *European Journal of Environmental and*  
698 *Civil Engineering*. 2015;19(10):1216-33.  
699 [59] Neville AM. *Properties of concrete*: John Wiley & Sons; 1995.

700

701